DANMARKS OG GRØNLANDS GEOLOGISKE UNDERSØGELSE RAPPORT 2005/16

Rock physics analysis of velocity differences in the chalks of wells Jette-1 and Isak-1

A contribution to the Chalk Background Velocity project

Gary Mavko & Peter Japsen

GEOLOGICAL SURVEY OF DENMARK AND GREENLAND
MINISTRY OF THE ENVIRONMENT

G E U S

DANMARKS OG GRØNLANDS GEOLOGISKE UNDERSØGELSE RAPPORT 2005/16

Rock physics analysis of velocity differences in the chalks of wells Jette-1 and Isak-1

A contribution to the Chalk Background Velocity project

The Chalk Background Velocity project is funded by the South Arne Group

Gary Mavko[1] & Peter Japsen[2]

[1]Stanford University, [2] GEUS

GEOLOGICAL SURVEY OF DENMARK AND GREENLAND
MINISTRY OF THE ENVIRONMENT

GEUS

Contents

Introduction – basic observations

In this note we discuss observations of P-wave sonic velocity differences between chalk intervals of the Jette-1 and Isak-1 wells. Questions of interest are, why are P-wave velocities higher in Jette-1 than in Isak-1? Why is the Vp/Vs ratio lower in Jette-1? We will show with rock physics models that these are consistent with different pore stiffnesses, though the mechanism for generating different pore stiffness is not clear.

Figure 1 compares well logs from the two wells. In both, the Ekofisk Formation is highlighted in red, the Tor Formation in blue, and the Hod Formation in green. The gamma ray log suggests differences between the two wells. In both wells, the Ekofisk tends to have relatively higher gamma ray than the cleaner Tor Formation. In Isak-1, the gamma ray in the Hod is comparable to the Tor, while in Jette-1 the gamma ray is significantly higher in the Hod than in the Tor. Overall, the gamma ray has significantly lower values in Jette-1 than in Isak-1, though the gamma ray is more variable in Jette-1 than in Isak-1, at least in the Ekofisk and Hod Formations.

Figure 2 shows sonic Vp vs. density porosity (Phi) for the Ekofisk, Tor, and Hod Formations in the two wells. For the Ekofisk and Tor Formations, we observe a wider range of porosities in Jette-1 than in Isak-1. Also, at a given porosity, the P-wave velocities in Jette-1 are higher than in Isak-1, for all formations. We also observe quite different velocity-porosity trends for the three formations. In Ekofisk, the velocity-porosity trend has a very low slope; the Tor slope is steeper; and the Hod slope is steeper still, though in Jette-1 the Hod slope is not so evident.

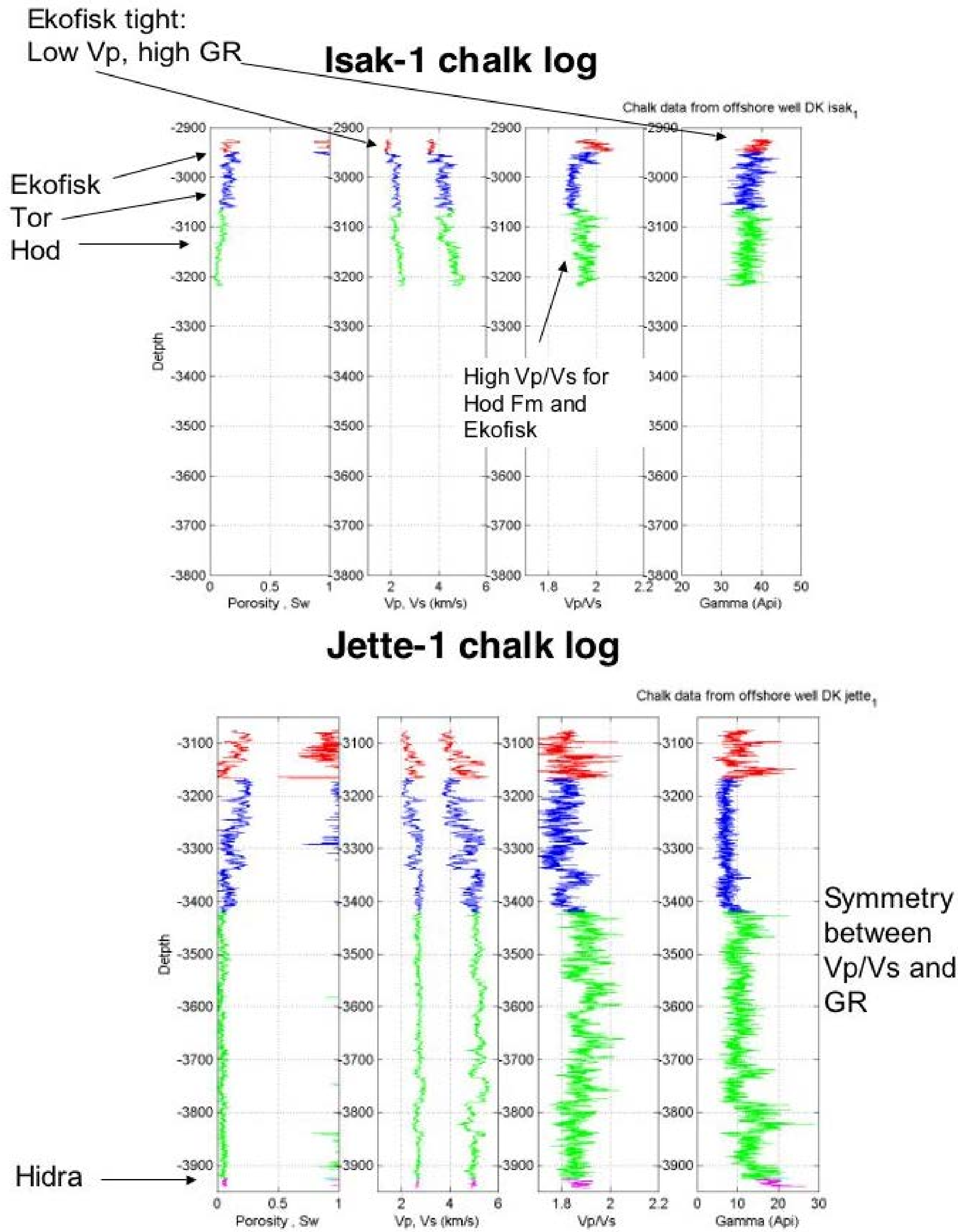

Figure 1. *Logs in Isak-1 and Jette-1. Ekofisk Formation is highlighted in red, Tor in blue, and Hod in green.*

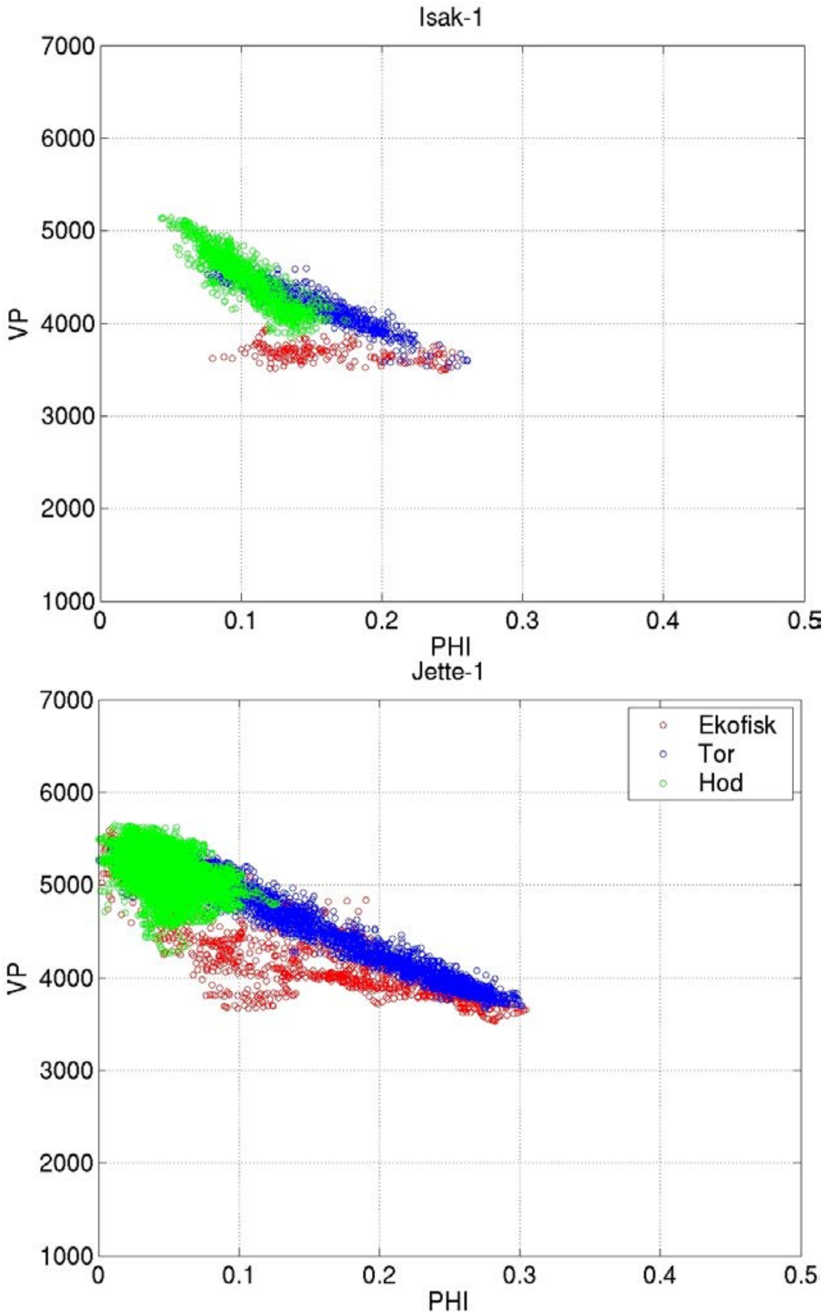

Figure 2. *Log P-wave sonic velocity vs. density porosity (Phi) in Isak-1 and Jette-1. Ekofisk Formation is highlighted in red, Tor in blue, and Hod in green.*

Figure 3 compares Vp/Vs ratio vs. Acoustic Impedance in Isak-1 and Jette-1. For the Ekofisk and Tor Formations, we observe a wider range of acoustic impedance in Jette-1 than in Isak-1. This mimics the porosity variation in Figure 2, since porosity and impedance tend to be highly correlated. At a given acoustic impedance, the Vp/Vs ratios in Jette-1 are lower than in Isak-1, for all formations, even though in Figure 2 we observed that Vp was higher in Jette-1.

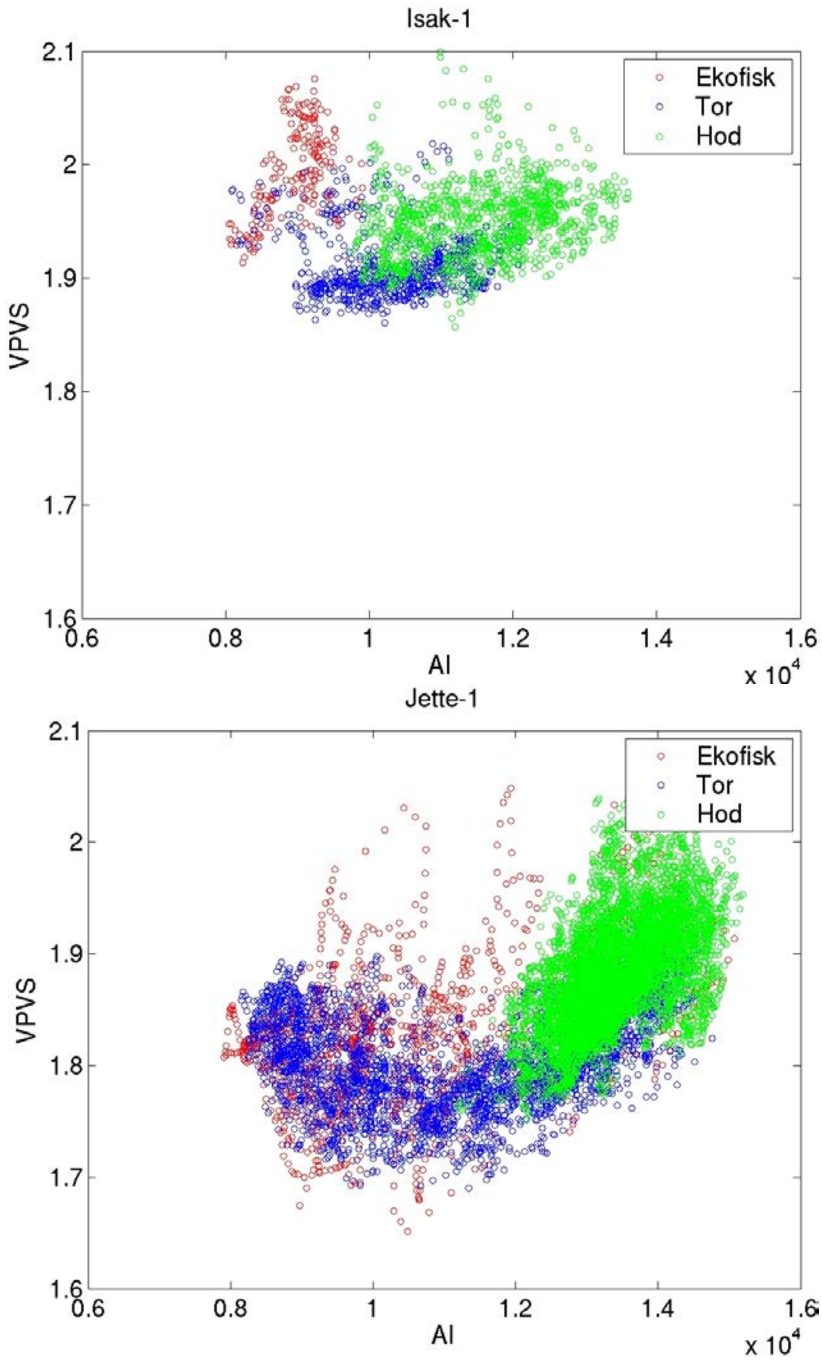

Figure 3. *Log sonic Vp/Vs ratio vs. acoustic impedance in Isak-1 and Jette-1. Ekofisk Formation is highlighted in red, Tor in blue, and Hod in green.*

Figure 4 compares sonic Vp vs. Vs in Isak-1 and Jette-1. The empirical Greenberg-Castagna (1992) lines for water-saturated sandstone (black line), shale (blue line), dolomite (magenta line) and limestone (green line) are shown for comparison. We also show a gas-saturated limestone line (dashed green), calculated from the water line using the Gassmann (1951) relations. Although none of the curves were developed explicitly for chalks, we see that the Jette-1 data mimic the limestone trend.

For each of the Greenberg-Castagna lithologic curves, the upper right extent can be interpreted as approximately the mineral point, at zero porosity. For pure calcite, this would correspond to (Vp=6370 m/s, Vs=3330 m/s). (Strictly , the Greenberg-Castagna curves do not pass exactly through this point. The reason is that they are empirical fits to data, and none of those data came close to zero porosity.) Moving to the lower left along each Greenberg-Castagna curve corresponds to increasing total porosity. The left-most intercept, at Vs=0 can be thought of as critical porosity, where the rock is falling apart. (Again, the precise Vp intercept value of the Greenberg-Castagna lines is not exactly what we would expect for a calcite-water suspension at critical porosity; the explanation again is that this high porosity limit is an extrapolation of the empirical Greenberg-Castagna curves beyond their range of validity.)

We observe in Figure 4 that the data from Isak-1 fall systematically above the Greenberg-Castagna carbonate line, while the data from Jette-1 fall along the line. That is, the Isak-1 data have systematically higher Vp/Vs ratios for all formations than the Jette-1 data. As discussed in later, this difference in Vp/Vs ratio appears to be consistent with rock textural or mineralogic differences between the two wells.

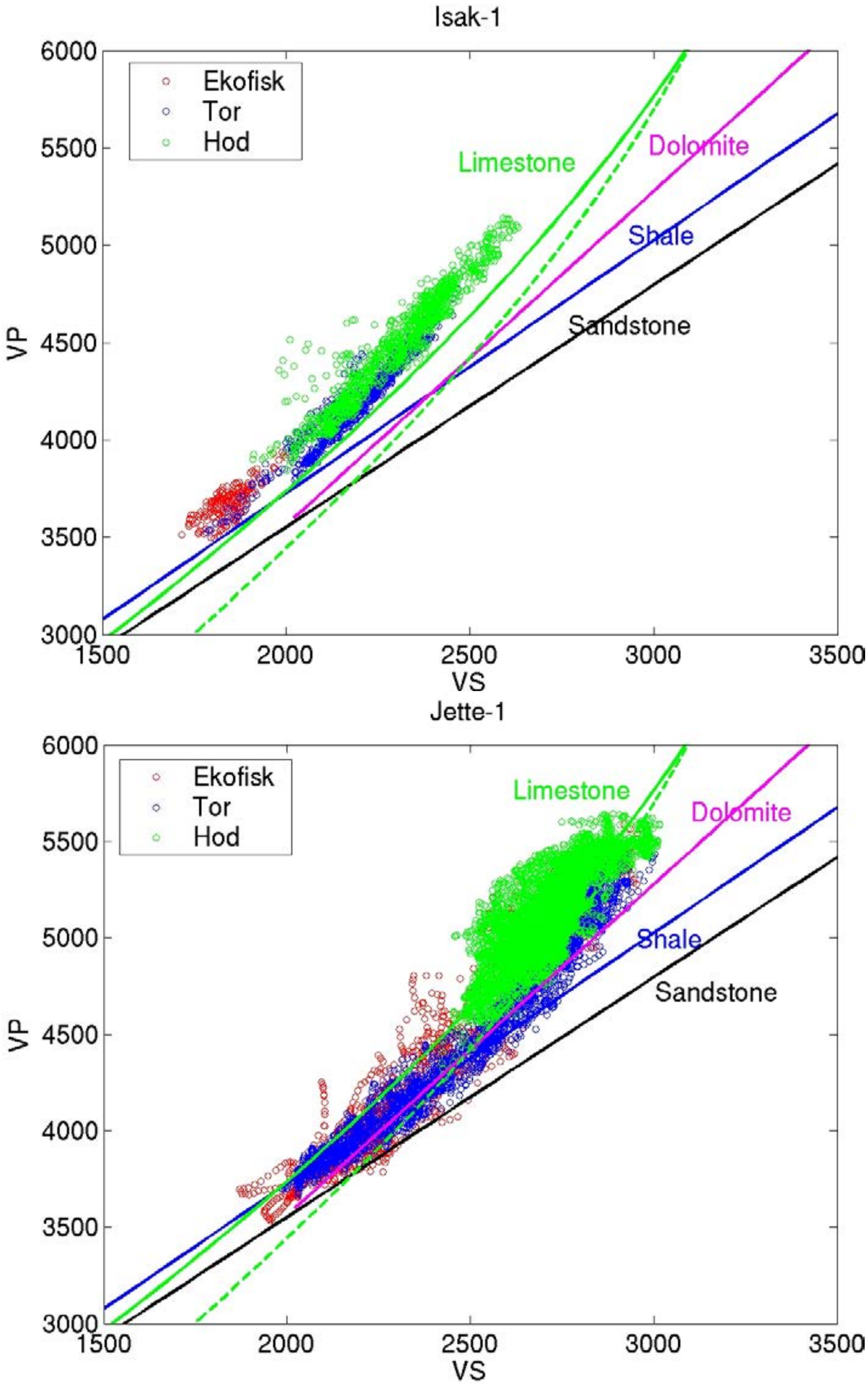

Figure 4. *Log sonic Vp vs. Vs in Isak-1 and Jette-1. Ekofisk Formation is highlighted in red, Tor in blue, and Hod in green. Greenberg-Castagna lines are shown for comparison.*

Rock physics modeling

In this section, we analyze the observations of Figures 2-4 by comparing them with rock physics models. One set of models represents the pore space as a collection of ellipsoidal inclusions, ranging from flat penny-shaped cracks to spherical pores. The equations that we implement are for the self-consistent formulation of Berryman (1995). The effective rock bulk and shear moduli of an N-phase composite are given by:

$$\sum_{i=1}^{N} x_i (K_i - K^*_{SC}) P^{*i} = 0$$

$$\sum_{i=1}^{N} x_i (\mu_i - \mu^*_{SC}) Q^{*i} = 0$$

where i refers to the *ith* material, x_i its volume fraction, P and Q are geometric factors given in Table 1, and the superscript ^{*i} on P and Q indicates that the factors are for an inclusion of material i in a background medium with self-consistent effective moduli K^*_{SC} and μ^*_{SC}. These equations are coupled and must be solved by simultaneous iteration.

In the modeling, spherical pores are represented with an aspect ratio of 1; these are the stiffest possible shapes, leading to high velocities for a given porosity. Successively smaller aspect ratios represent flattened spherical pores (oblate spheroids), which are successively more compliant. Aspect ratios less than about 0.1 are often referred to as “penny-shaped” cracks. In our application, we assume two phases, calcite and water.

In using these inclusion models, it is important to remember that they are quite idealized, and should not be interpreted too literally. In real rocks there are no ellipsoidal pores. Also, the ellipsoidal models do not explicitly allow for pore connectivity. Nevertheless, these models are useful elastic analogs, and we believe that the trends predicted by them, such as from stiffer pores to more compliant pores, are valid. In our discussion below, the fact that Isak-1 data are consistent with a penny-shaped crack model does not mean that there must be cracks in the rocks. Poorly cemented, compliant grain contacts will yield the same elastic behavior.

Table 1. *Coefficients P and Q for some specific shapes. The subscripts m and i refer to the background and inclusion materials [from Berryman (1995)].*

Inclusion shape	P^{mi}	Q^{mi}
Spheres	$\dfrac{K_m + \frac{4}{3}\mu_m}{K_i + \frac{4}{3}\mu_m}$	$\dfrac{\mu_m + \zeta_m}{\mu_i + \zeta_m}$
Needles	$\dfrac{K_m + \mu_m + \frac{1}{3}\mu_i}{K_i + \mu_m + \frac{1}{3}\mu_i}$	$\dfrac{1}{5}\left(\dfrac{4\mu_m}{\mu_m + \mu_i} + 2\dfrac{\mu_m + \gamma_m}{\mu_i + \gamma_m} + \dfrac{K_i + \frac{4}{3}\mu_m}{K_i + \mu_m + \frac{1}{3}\mu_i}\right)$
Disks	$\dfrac{K_m + \frac{4}{3}\mu_i}{K_i + \frac{4}{3}\mu_i}$	$\dfrac{\mu_m + \zeta_i}{\mu_i + \zeta_i}$
Penny cracks	$\dfrac{K_m + \frac{4}{3}\mu_i}{K_i + \frac{4}{3}\mu_i + \pi\alpha\beta_m}$	$\dfrac{1}{5}\left(1 + \dfrac{8\mu_m}{4\mu_i + \pi\alpha(\mu_m + 2\beta_m)} + 2\dfrac{K_i + \frac{2}{3}(\mu_i + \mu_m)}{K_i + \frac{4}{3}\mu_i + \pi\alpha\beta_m}\right)$

$$\beta = \mu\frac{(3K+\mu)}{(3K+4\mu)} \qquad \gamma = \mu\frac{(3K+\mu)}{(3K+7\mu)} \qquad \zeta = \frac{\mu}{6}\,\frac{(9K+8\mu)}{(K+2\mu)}$$

Effect of mineral properties on inclusion model predictions

When comparing theoretical curves with well log data, we find that the results are very sensitive to the assumed mineral properties. Figure 5 shows plots of Vp vs. Vs, Vp vs. Phi, and Vs vs. Phi for the Ekofisk, Tor, and Hod Formations of Isak-1. Superimposed are the predictions of the ellipsoidal inclusion model, for average pore aspect ratios of [1, 0.3, 0.1, 0.03, 0.01]. For these curves, we assumed mineral bulk modulus, $K = 65\,GPa$, shear modulus, $\mu = 27\,GPa$, and density, $\rho = 2.71\,g/cm^3$. From the top two plots, it appears that most of the data fall between aspect ratios ~.03 and ~02. Looking closer, we see that the Vp-Phi plot (top) shows data extending to about half way between the curves for aspect ratios 0.1 and 0.3; in contrast, the Vs-Phi plot (middle) shows data falling only slightly above the curve for aspect ratio 0.1. Hence, there is an inconsistency with the model – it does not make physical sense that the P-waves are seeing stiffer aspect ratios than the S-waves. The inconsistency is even more obvious in the plot of Vp-Vs (bottom).

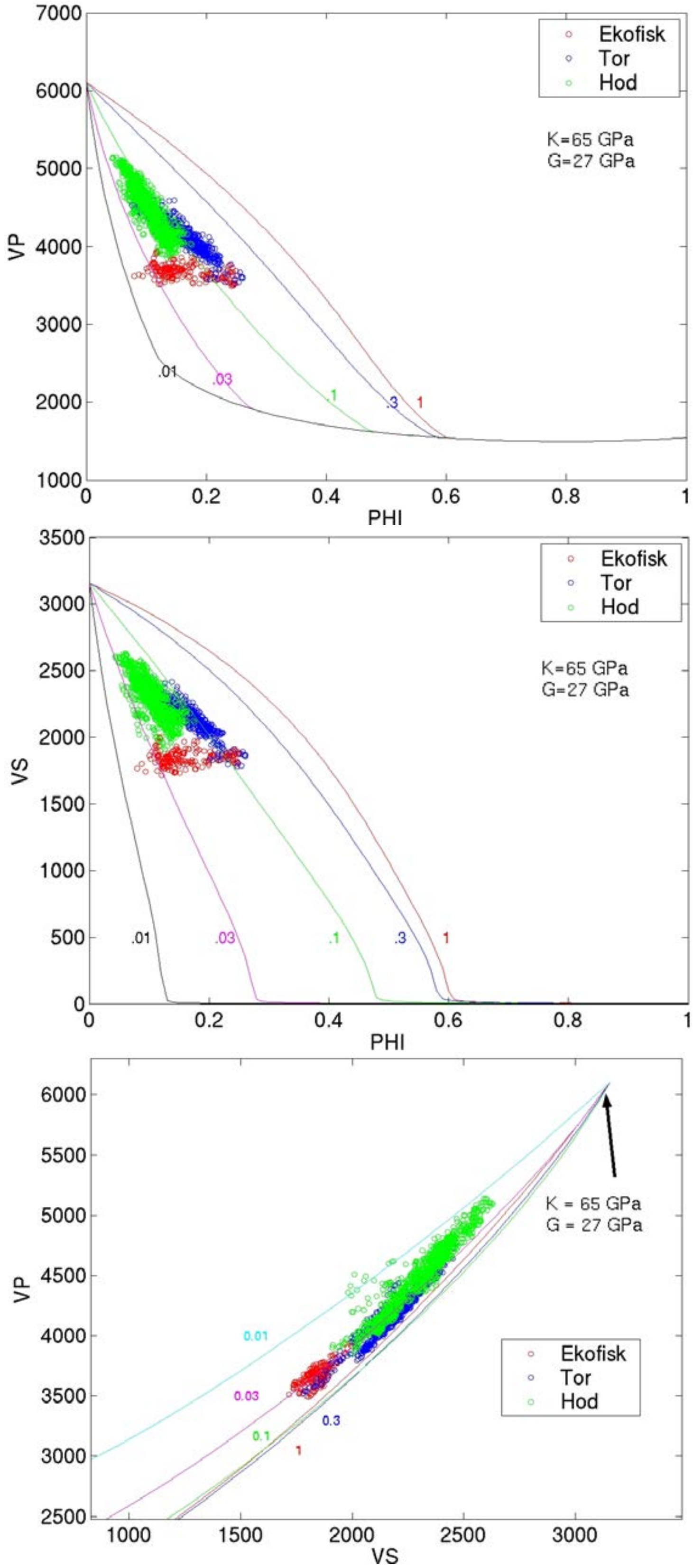

Figure 5. *Plots for the Ekofisk, Tor, and Hod Formations of Isak-1, showing the model inconsistency resulting from a poor choice of mineral properties.*

Note that data from the Hod Formation (green) extend to very small aspect ratios, ~0.01, while in the Vp-Phi and Vs-Phi plots, the Hod always falls above the curve for 0.03. One way to explain this discrepancy is that the Poisson's ratio of the elastic mineral used for modeling is not consistent with the observed Poisson's ratio of the porous rocks.

Figure 6 shows the same type of plots as in Figure 5, but now with mineral properties adjusted to $K = 67 GPa$, $\mu = 23 GPa$, and density, $\rho = 2.71 g/cm^3$. The moduli were adjusted empirically to find model predictions consistent with both P- and S-wave velocity data. We now observe that the plots of Vp vs. Phi (top) and Vs vs. Phi (middle) show data falling consistently in the aspect ratio range ~.03-.2. The plot of Vp vs. Vs (bottom) shows essentially the same range. (In this plot the curves for larger aspect ratios (.1, .3, and 1) cluster very close together, so it is difficult to conclude much about the higher end aspect ratio suggested by the data.) Hence, by adjusting the mineral moduli, we can find model aspect ratios that are consistent with both P- and S-wave velocities at Isak-1. It is interesting that this single adjustment improved the consistency for all three formations, even though the formations have different textures, pore shapes, and Poisson's ratios.

Figure 7 shows the same type of plots as in Figures 5 and 6, but now for Jette-1. Here, model consistency with both Vp and Vs requires a different set of mineral properties, $K = 60 GPa$, $\mu = 27 GPa$, and density, $\rho = 2.71 g/cm^3$.

In summary, inference of pore shapes corresponding to the log data, based on the ellipsoidal inclusion model is very sensitive to the choice of mineral properties. We observed in Figures 5 and 6 for well Isak-1 that adjusting the moduli from ($K = 65 GPa, \mu = 27 GPa$) to ($K = 67 GPa, \mu = 23 GPa$) has a large effect on the consistency of the models with P- and S-wave data. This adjustment caused a change in mineral Vp of only about ~1%, but a change in mineral Vs of ~ 7%.

Similarly, model consistency required a change in mineral moduli between Isak-1 and Jette-1. Mineral Vp at Jette-1 is about 1% slower than at Isak-1, while mineral Vs at Jette-1 is about 7% faster than at Isak-1.

It is difficult to know how much of this discrepancy is a limitation of the idealized ellipsoidal inclusion model. Nevertheless, the Vp/Vs behavior of the data from the two wells shows different trends, with Vp/Vs at Jette-1 generally lower than Isak-1.

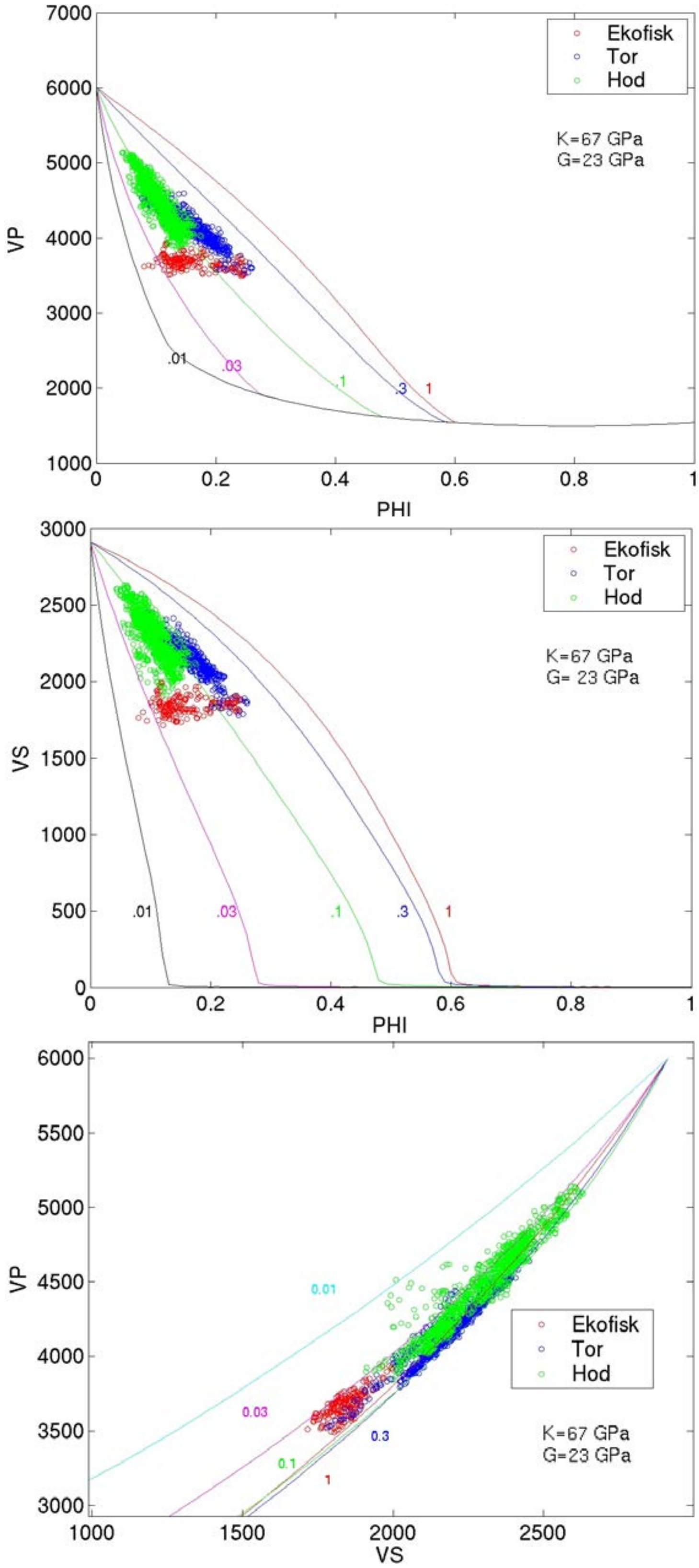

Figure 6. *Plots for the Ekofisk, Tor, and Hod Formations of Isak-1, showing improved model consistency resulting from adjusted mineral properties. Mineral bulk and shear moduli used in the modeling are labeled in the figures.*

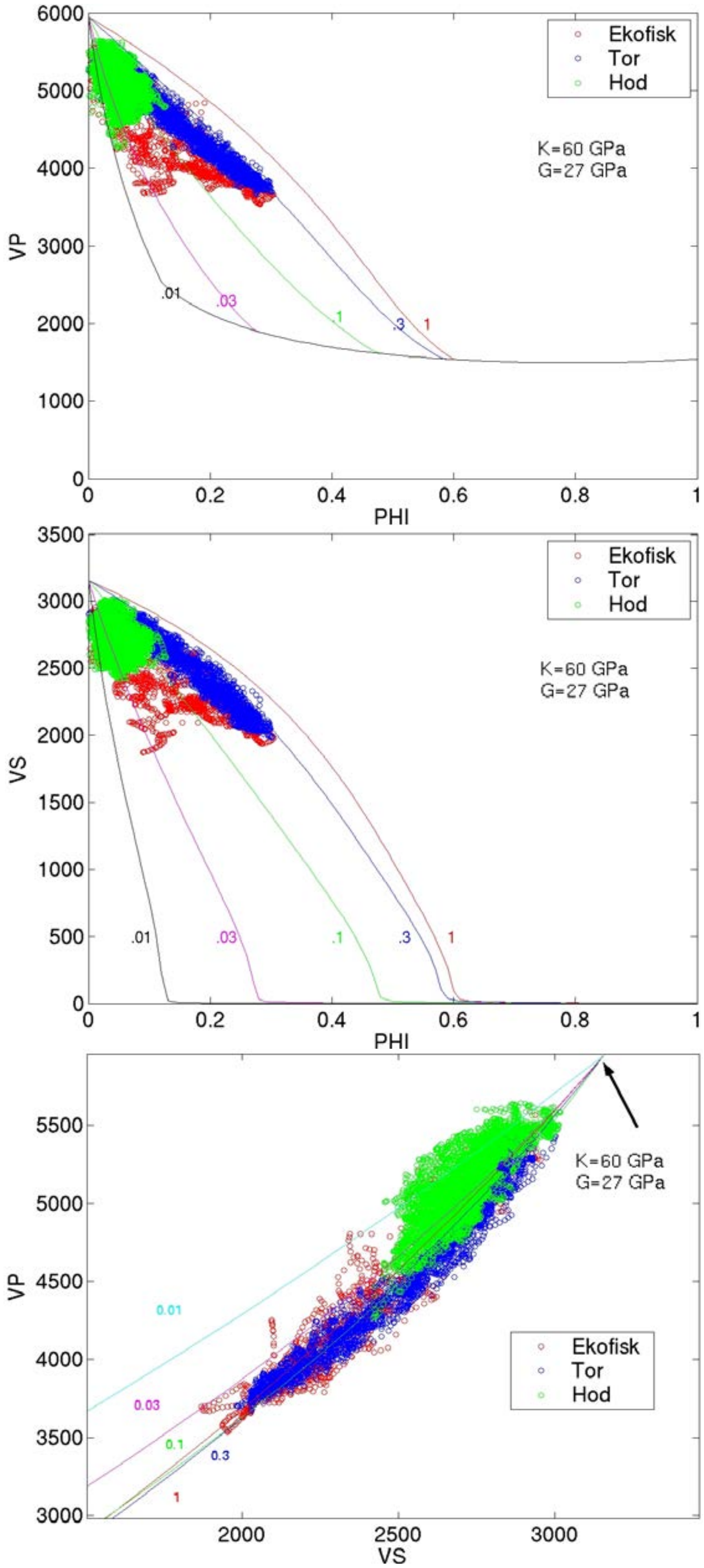

Figure 7. *Plots for the Ekofisk, Tor, and Hod Formations of Jette-1, showing good model consistency resulting from adjusted mineral properties. Mineral bulk and shear moduli used in the modeling are labeled in the figures.*

Comparison of Jette-1 and Isak-1 in the velocity-porosity planes

Figure 8 compares plots of sonic Vp vs. Phi and Vs vs. Phi for the Ekofisk, Tor, and Hod Formations in Isak-1 and Jette-1. Predictions of the ellipsoidal inclusion model are superimposed, for average pore aspect ratios of [1, 0.3, 0.1, 0.03, 0.01]. As discussed above, slightly different mineral moduli were used for each well, though the mineral Vp is virtually the same. The comparison suggests that the rocks from Jette-1 appear to span a much larger range of pore shapes than the rocks in Isak-1 (although we will show below that this is likely related to clay content). Rocks of the Tor Formation (blue) show the cleanest trend for both wells, and in Jette-1, the Tor seems to have significantly rounder, stiffer pores than in Isak-1. The Hod Formation in Isak-1 shows a very consistent Vp-Phi trend, with aspect ratios between .03-.1, while the Hod Formation in Jette-1 is quite variable, spanning from soft (~.01) to stiff (~1) pores (again, likely a clay effect). The Ekofisk Formation shows a range of pore aspect ratios in both wells, but the range is much larger in Jette-1, especially extending to stiffer pore shapes, similar to the Tor.

Figure 9 compares plots of sonic Vp vs. Vs for the Ekofisk, Tor, and Hod Formations in Isak-1 and Jette-1. Predictions of the ellipsoidal inclusion model are superimposed. Once again the Tor Formation in Jette-1 appears to have stiffer pore space (large aspect ratios) than in Isak-1, though in these axes the large aspect ratios are difficult to resolve.

What processes can lead to differences in pore stiffness? One hypothesis is that earlier in their burial histories, rocks from both the Isak-1 and Jette-1 wells had similar microstructures, with compliant grain-to-grain contacts. As time went on, rocks in the Ekofisk and Tor Formations of Jette-1 gained more cement preferentially deposited at the grain contacts. This would account for some stiffer rocks in the Tor and Ekofisk Formations, but it does not explain the overall larger range of porosities and the larger range of pore stiffnesses in Jette-1. A second hypothesis is that rocks in the different wells suffered different amounts of strain or pore pressure, which created microcracks resulting in a softer pore space. A third hypothesis is that we are seeing elastic effects of clay in the dirtier Ekofisk and Hod Formations.

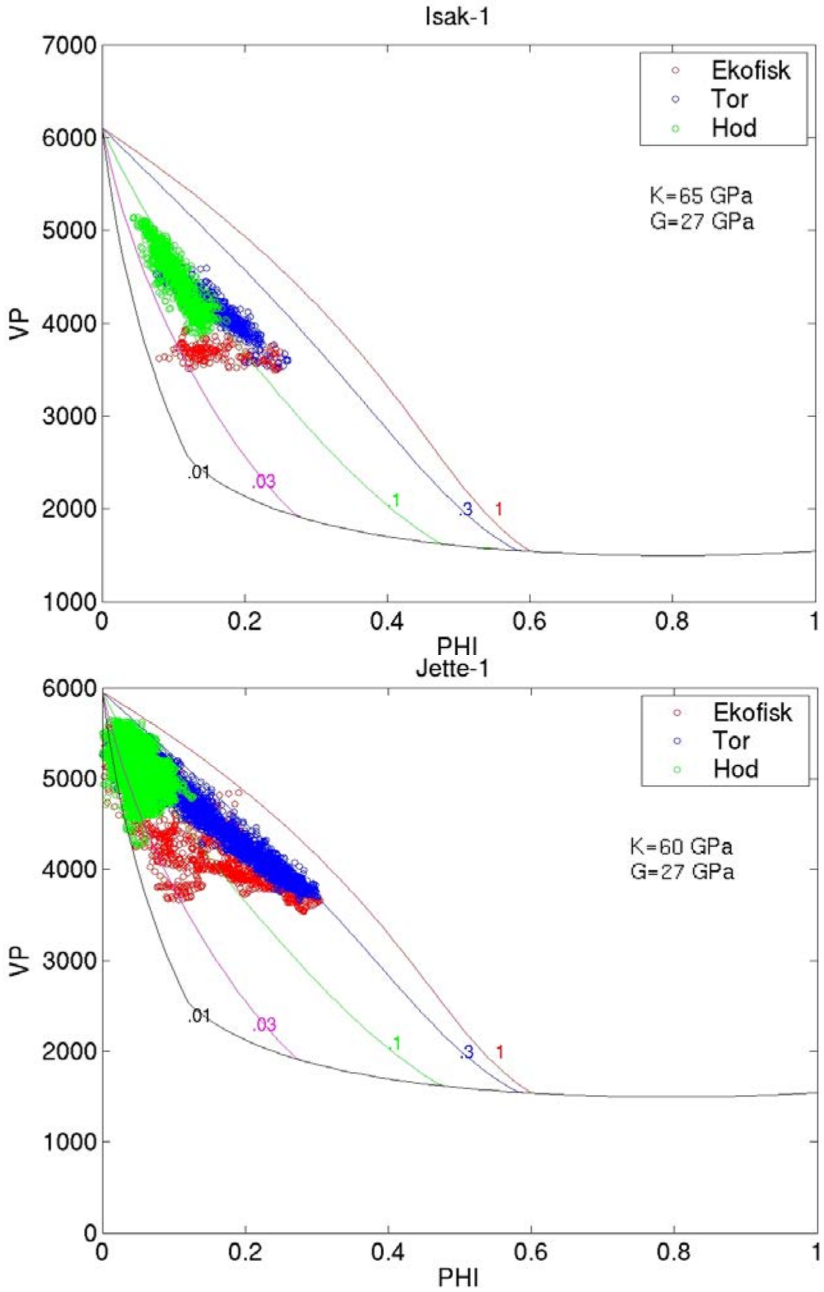

Figure 8. *Comparison of Vp vs. porosity in Isak-1 (top) and Jette-1 (bottom). Predictions of a rock physics model representing pores of various aspect ratios (numbers next to the various curves) are superimposed. Ekofisk Formation is highlighted in red, Tor in blue, and Hod in green.*

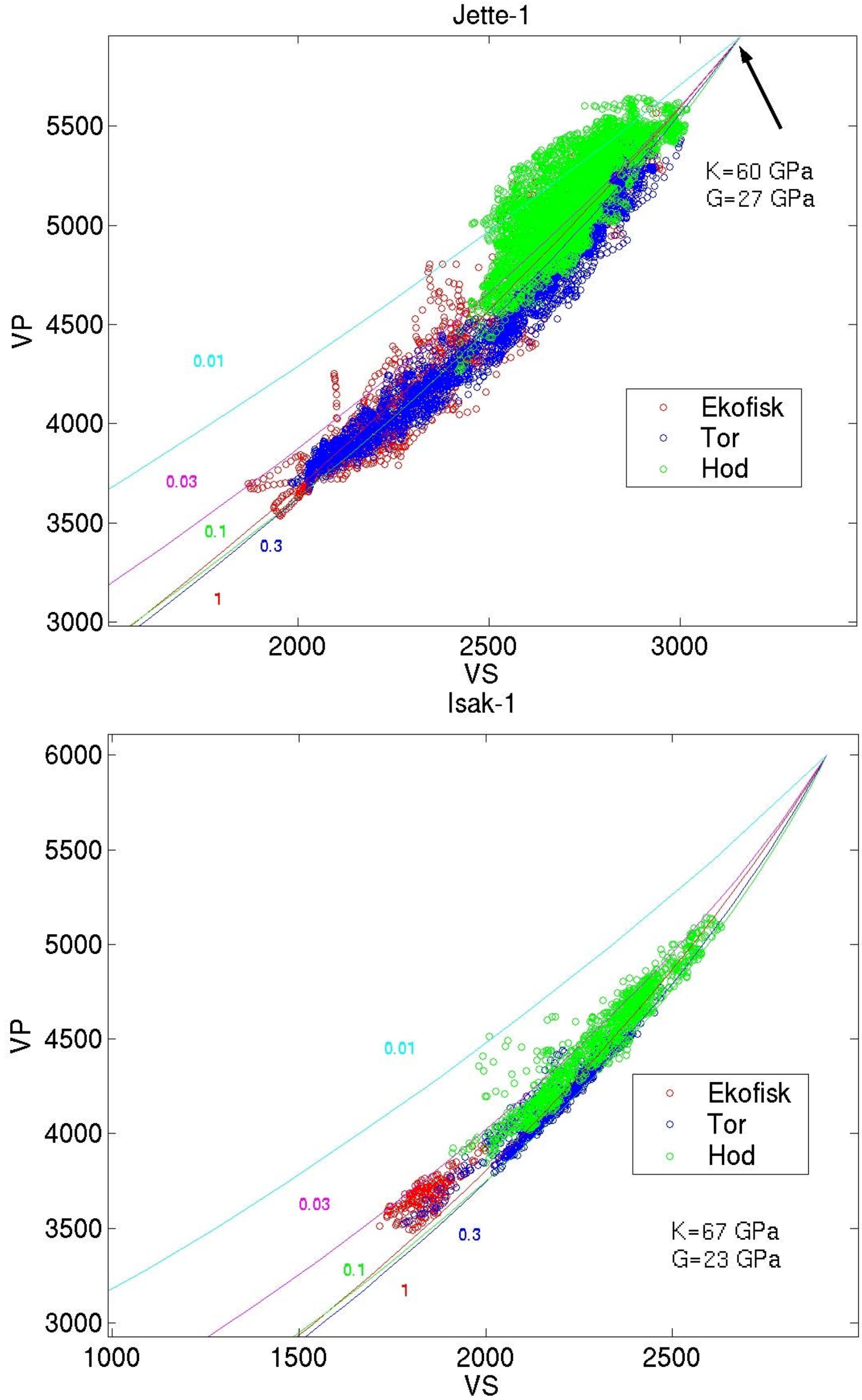

Figure 9. *Log sonic Vp vs. Vs in Isak-1 and Jette-1. Predictions of a rock physics model representing pores of various aspect ratios (numbers next to the various curves) are superimposed. Ekofisk Formation is highlighted in red, Tor in blue, and Hod in green.*

Interpretations of differing mineral properties

In the previous sections we illustrated that consistency between the well log data and the ellipsoidal inclusion models indicated different mineral properties in Isak-1 vs. Jette-1. For reference, the parameters that we used are shown in the table below.

Mineral properties used in elastic models of wells Isak-1 and Jette-1

	Bulk Modulus (GPa)	Shear Modulus (GPa)	Density (g/cm3)
Isak-1	67	23	3.31
Jette-1	60	27	3.31

What might account for this difference? One scenario that we consider is that well Jette-1 has more quartz present in the mineral matrix, possibly the result of precipitation from pore fluids after deposition.

To test this idea, we modeled the average elastic properties for mixtures of quartz and calcite, as shown in Figure 10. In the figure, we plot average mineral bulk modulus vs. average mineral shear modulus. No porosity is included in the modeling; we are only considering the average properties of the mineral matrix. The average moduli were computed in two different ways. The thin black curves show the upper and lower Hashin-Shtrikman bounds. All mixtures of quartz and calcite, regardless of the way they are geometrically arranged, must fall between these two bounds. The bounds are very close to each other, because the properties of calcite and quartz end members are elastically similar – within a factor of two.

The red line shows the results of assuming a composite of equant grains of the two minerals, computed using the ellipsoidal inclusion model. As expected for a physically realizable model, the results fall between the Hashin-Shtrikman bounds. We found that the results were virtually independent of the assumed aspect ratios of the quartz and calcite, again the result of quartz and calcite being elastically similar. In both models, we took the properties of the Isak-1 mineral as the calcite end member (point on the upper left of the graph, labeled Quartz fraction = 0); the properties of quartz were assumed to be $K = 36\,GPa$ and $\mu = 45\,GPa$ (point on the lower right of the graph, label Quartz fraction = 1). The properties for the Jette-1 mineral that we determined by trial and error in the previous section, are shown by a black dot. Note that in fact, it corresponds very closely to the theoretically expected value for a mixture of 80% calcite and 20% quartz.

A second observation that we discussed in Figures 6 and 7 is that the rocks in Jette-1 appear to have stiffer pores than in Isak-1. This again could be the result of quartz cementation, particularly if the quartz fills the thinnest cracks and grain contacts, resulting in a more rigid pore space.

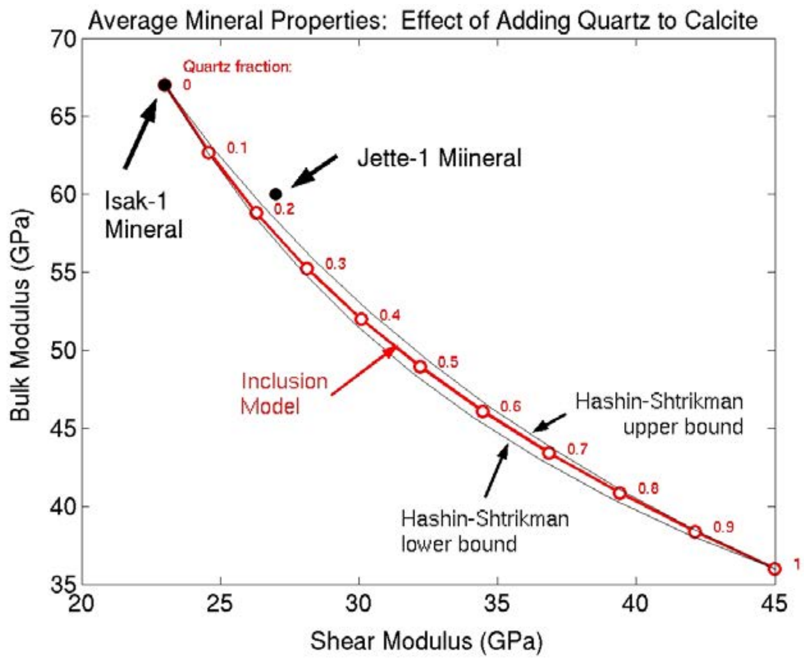

Figure 10. *Theoretical predictions of the average modulus of calcite and quartz mixed in different proportions. The point on the upper left is for pure calcite and on the lower right, pure quartz. Predictions of the Hashin-Shtrikman bounds and the elastic inclusion model give essentially the same result. The Jette-1 mineral is consistent with 20% quartz.*

Another aspect of the mineralogy is the effect of clay. In general, clay tends to soften both the bulk and shear moduli of rocks, and tends to increase the Vp/Vs ratio. One of the observations of Figure 7 is that the Hod Formation in Jette-1 has a large apparent range of aspect ratios, and a large Vp/Vs ratio. We also observed in Figure 7 that the data in the Vp vs. Vs plane have a large scatter relative to the ellipsoidal model curves.

Figure 11 shows the data from Jette-1, now color-coded by gamma ray. The data are shown for the Ekofisk, Tor, and Hod Formations together, as well as separately. The clean Tor Formation shows little variation with gamma ray. However, the clay-bearing Ekofisk and Hod Formations show a large variation in gamma ray, and a large variation in apparent aspect ratios. In fact, Figure 11 suggests that the data extending to the smallest aspect ratio curves are probably reflecting the presence of clay, rather than a systematic change in pore shape.

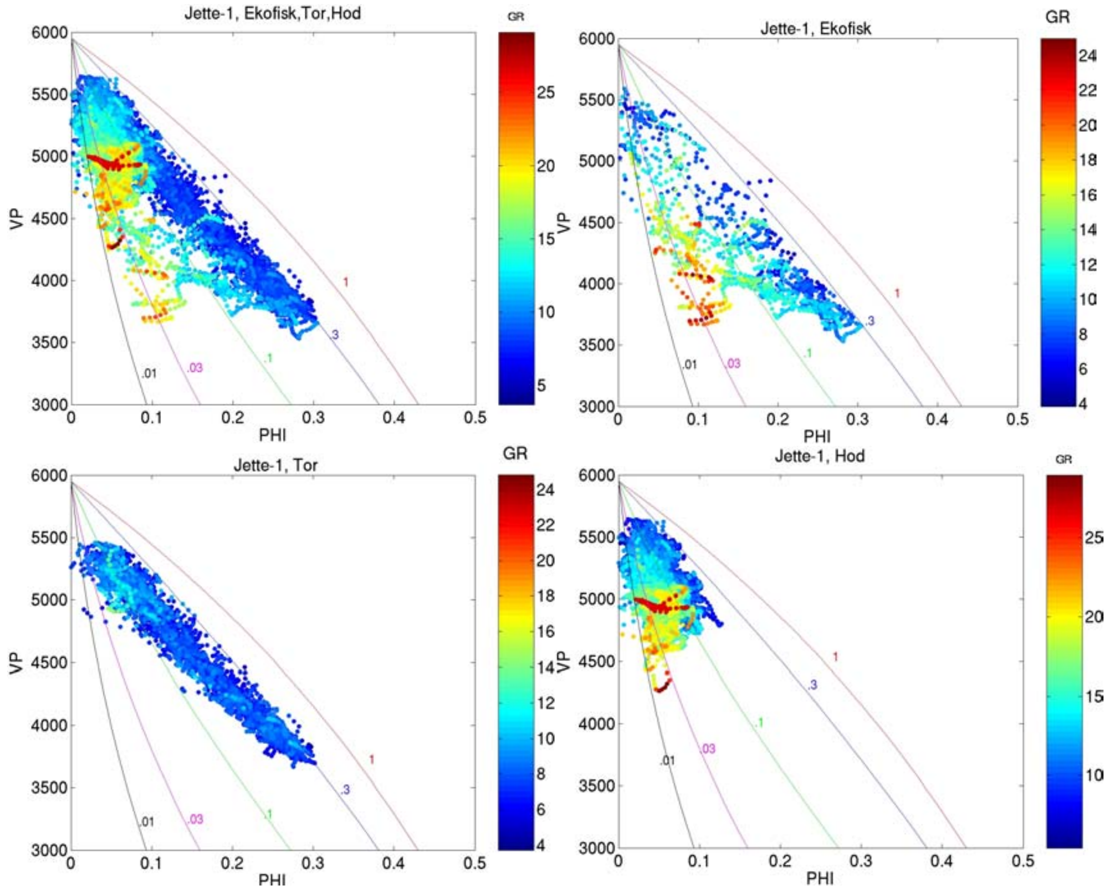

Figure 11. *Plots of Vp vs. Phi in Jette-1, color-coded by gamma ray. Plots of Ekofisk, Tor, and Hod Formations are shown together (upper left) and separately.*

Empirical models in the Vp-Vs plane

Additional insights into the effects of rock texture can be gotten by comparing Greenberg-Castagna curves for sand and limestone lithologies, as shown in Figure 12. Empirical studies on clastics almost always indicate a *linear* relation between Vp and Vs extending from the quartz mineral point, as illustrated by the blue Greenberg-Castagna sand line in Figure 12. In contrast, carbonates often show a quadratic relation, as illustrated by the *curved* green Greenberg-Castagna limestone line. A conceptual view of the corresponding rock textures is that sandstones are made from an assembly of *particles*, while limestones are calcite mineral, containing an assembly of *holes*.

Tsuneyama, et al. (2003) showed that, in contrast to most limestones, carbonate *grainstones* have Vp/Vs larger than expected from the usual Greenberg-Castagna curve; they found that grainstone Vp-Vs follows a straight line extending from the mineral point, as illustrated by the magenta line in Figure 12. Since grainstones can be thought of as an assembly of carbonate particles, texturally resembling a clastic, it is not surprising that the corresponding Vp-Vs relation is linear. In fact, we construct the grainstone line in Figure 12 by taking the sandstone line and scaling it by the ratio of calcite to quartz bulk and shear moduli.

Figure 13 shows Vp vs. Vs with the grainstone line (magenta) and Greenberg-Castagna carbonate line (green), similar to Figure 12. We now superimpose the Hashin-Shtrikman upper bound (red), computed for calcite ($K = 65\,GPa$, $\mu = 27\,GPa$, $\rho = 2.71\,g/cm^3$) and water ($K = 2.2\,GPa$, $\rho = 1.02\,g/cm^3$). We see that the curved Greenberg-Castagna line falls almost exactly along the upper bound, indicating that it represents essentially the stiffest possible pore space in calcite mineral. Points plotting anywhere above this line represent rocks with softer pore space.

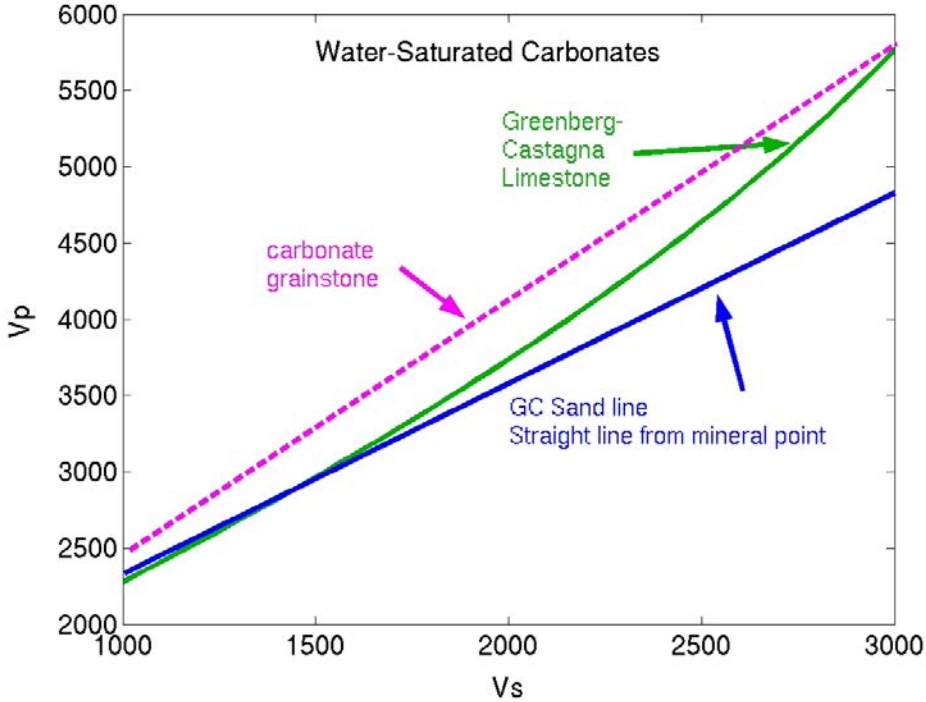

Figure 12. *Comparison of empirical Vp-Vs relations for sands and carbonates. The empirical Greenberg-Castagna line for sandstone is shown in blue, the Greenberg-Castagna curve for limestones is shown in green, and a carbonate grainstone line is shown in dashed magenta.*

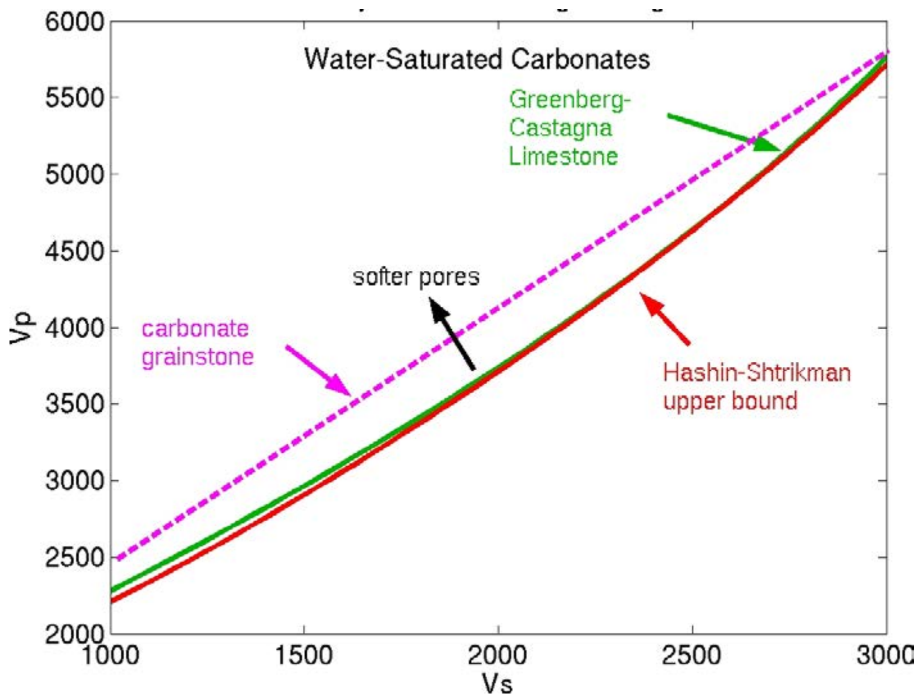

Figure 13. *Comparison of empirical Greenberg-Castagna curve for limestones with Hashin-Shtrikman upper bound.*

Figure 14 compares sonic Vp vs. Vs in Isak-1 and Jette-1, similar to Figure 4. The empirical Greenberg-Castagna (1992) line for limestone (dark green curve) is shown for comparison. We also show the carbonate grainstone line from Figure 12 (magenta; upper plot) and a gas-saturated line (dashed green; lower plot). We observe, as before, that the data from the Ekofisk and Tor in Jette-1 are fairly consistent with the limestone line, while data from Hod in Jette-1 and all formations in Isak-1 deviate in the direction of the grainstone line. This would suggest that a textural difference could account for the differences observed between the two wells.

Figure 15 compares data from Isak-1 and Jette-1, one formation at a time. The Greenberg-Castagna lines for water and gas-saturated limestones are shown for reference. In each case the rocks in Isak-1 have larger Vp/Vs ratio than the corresponding formation in Jette-1. Also striking is that in each case the rocks in Jette-1 tend to have higher velocities and span a larger range of velocities than the corresponding formations in Isak-1.

Figure 16 shows data for Isak-1 and Jette-1, color-coded by depth. In Isak-1, there is a fairly monotonic increase of velocities with depth. However in Jette-1, the depth variation is more complicated. Rocks from the shallower Ekofisk and Tor Formations span the entire range of velocities. Data from the Hod Formation fall in the upper half of the velocity range, though within the Hod, there is not a systematic increase of velocity with depth.
Figure 17 shows data from Isak-1 and Jette-1, again color-coded by depth. Ellipsoidal inclusion models are superimposed. In Isak-1, there is no apparent change of pore shape with depth, even though the velocities increase systematically with depth. This can correspond to a systematic decrease in porosity with depth, without a significant change in pore shape. In Jette-1, there is a stiffening of pore shape with depth within the Tor Formation,

and again within the Hod Formation. This stiffening within each of the formations seems to occur without a systematic decrease of porosity with depth.

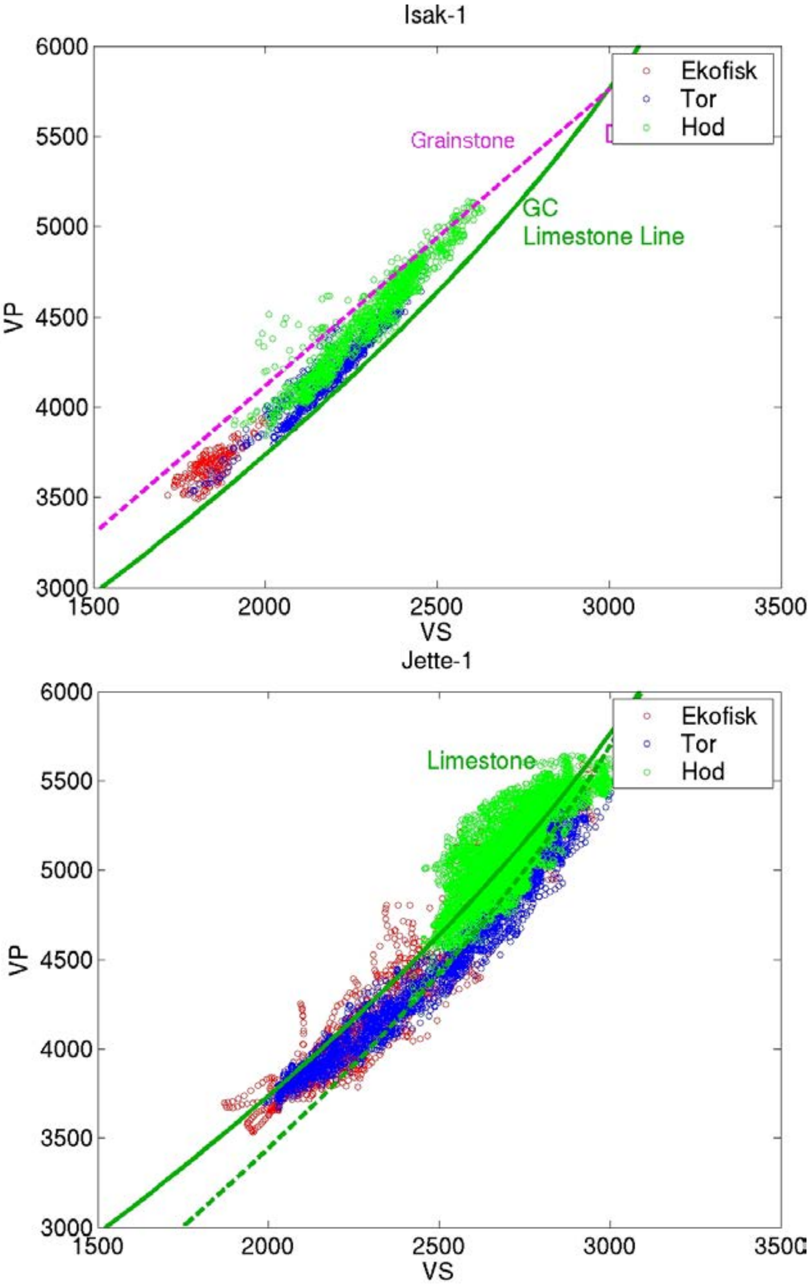

Figure 14. *Comparison of empirical Vp-Vs relations for sands and carbonates. The empirical Greenberg-Castagna curve for limestones is shown in dark green (water-solid, gas-dashed), and a carbonate grainstone line is shown in dashed magenta. Data from the Ekofisk Formation is shown in red; the Tor in blue; and the Hod in green.*

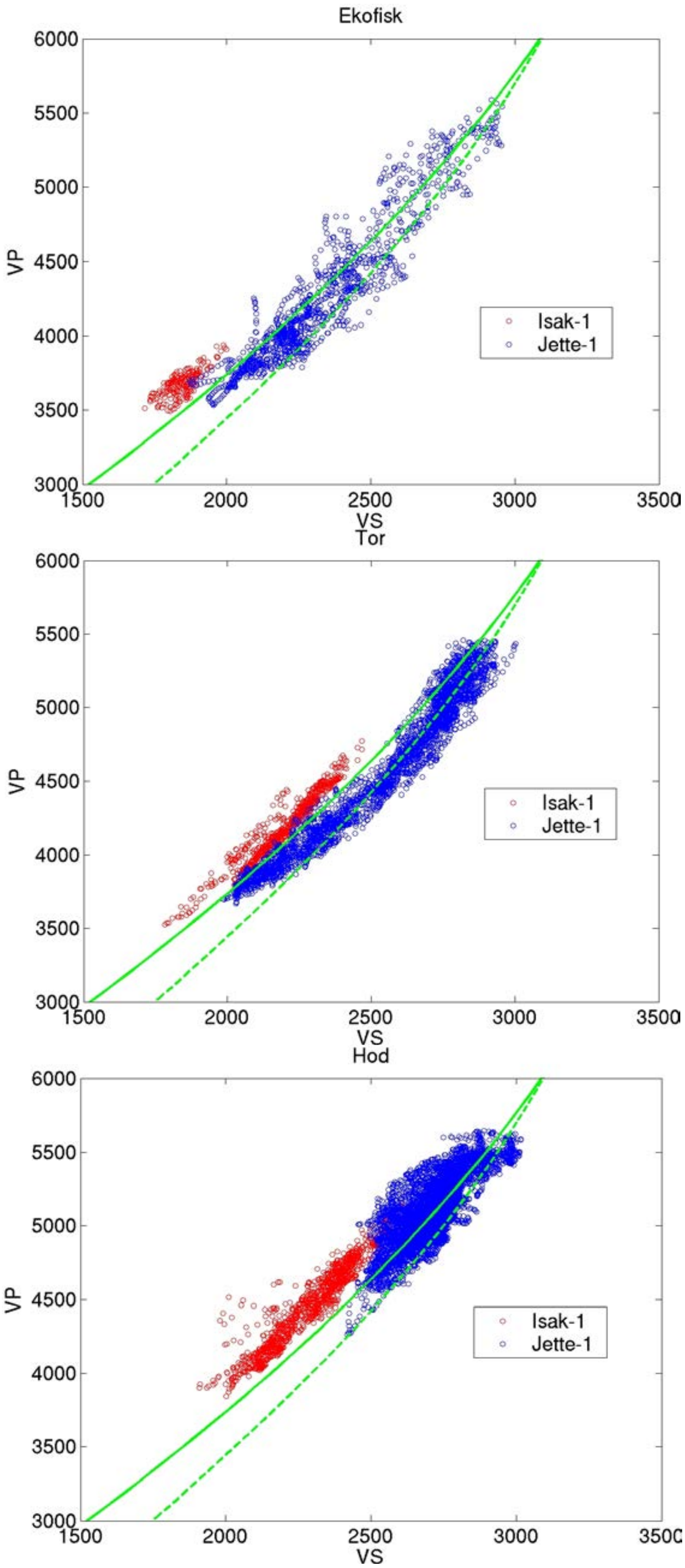

Figure 15. *Comparison Isak-1 and Jette-1, for each Formation. Greenberg-Castagna curves for limestones (water: solid; gas: dashed) are superimposed.*

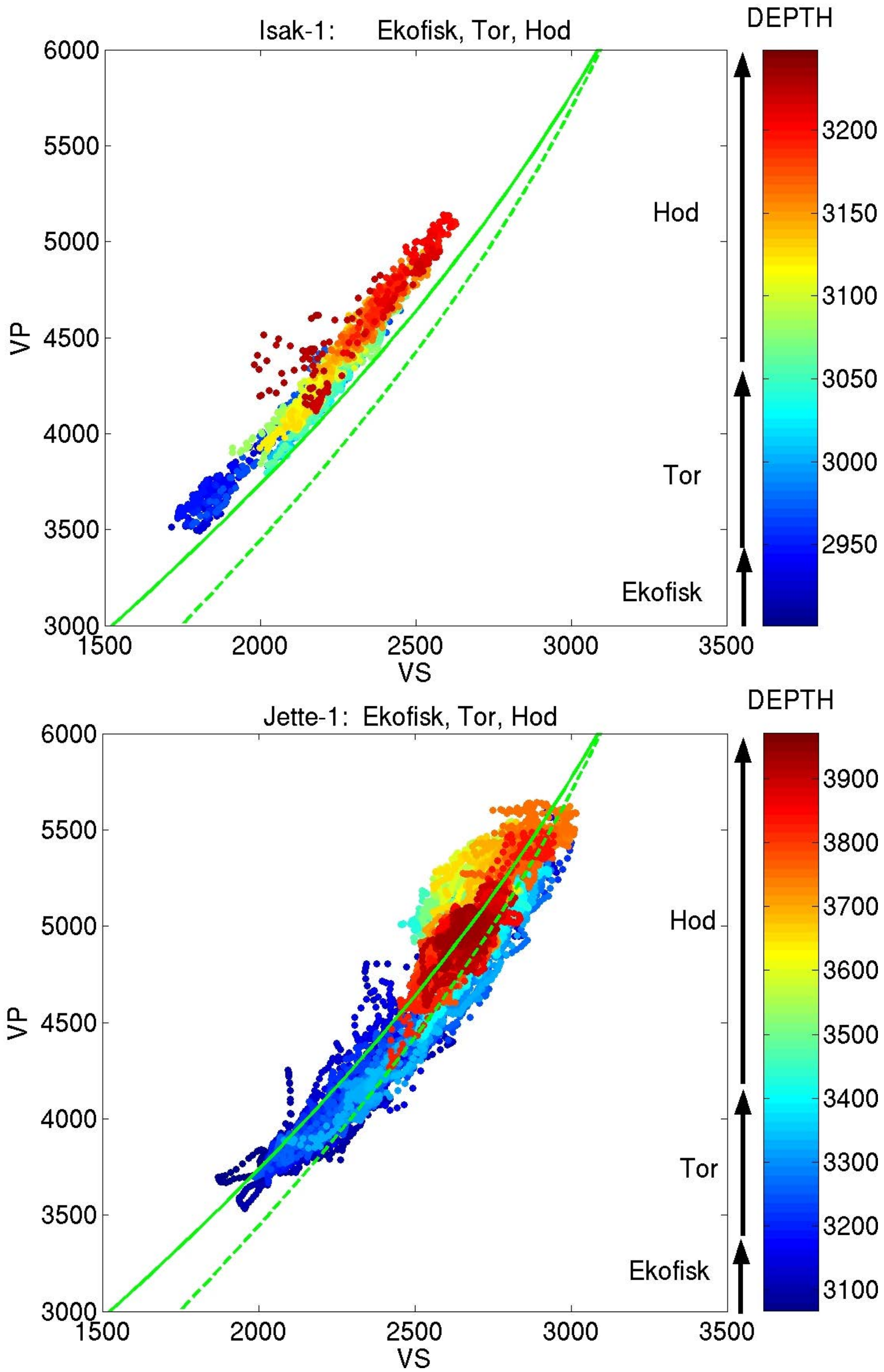

Figure 16. *Comparison Isak-1 and Jette-1, color-coded by depth. Greenberg-Castagna curves for limestones (water: solid; gas: dashed) are superimposed.*

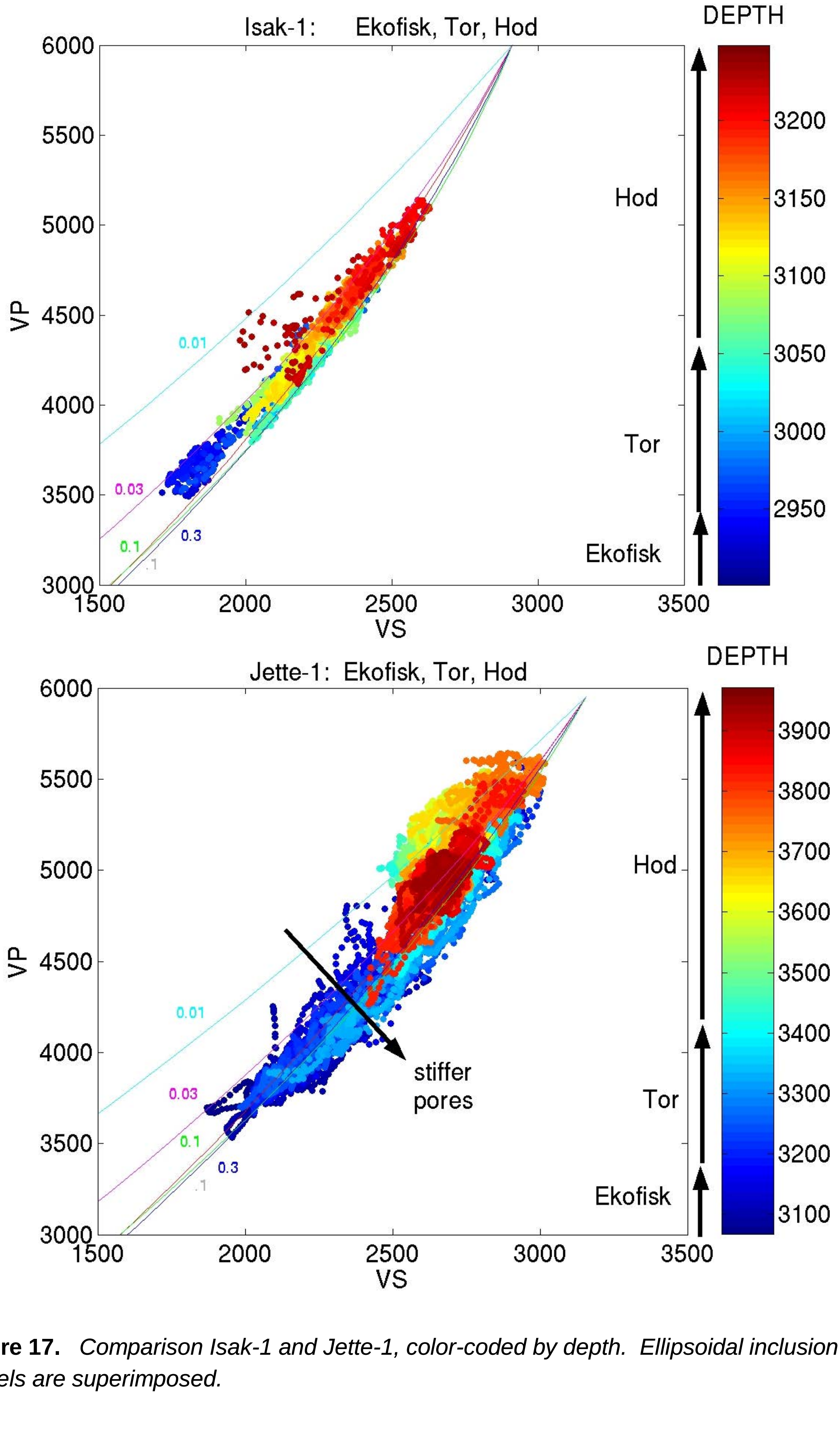

Figure 17. *Comparison Isak-1 and Jette-1, color-coded by depth. Ellipsoidal inclusion models are superimposed.*

The acoustic impedance – Poisson's ratio plane

Finally, we compare data from Isak-1 and Jette-1 plotted as acoustic impedance vs. VpVs ratio (Figure 18) and Poisson's ratio (Figure 19). Both planes highlight the differences in apparent pore stiffness and velocity that we have been discussing.

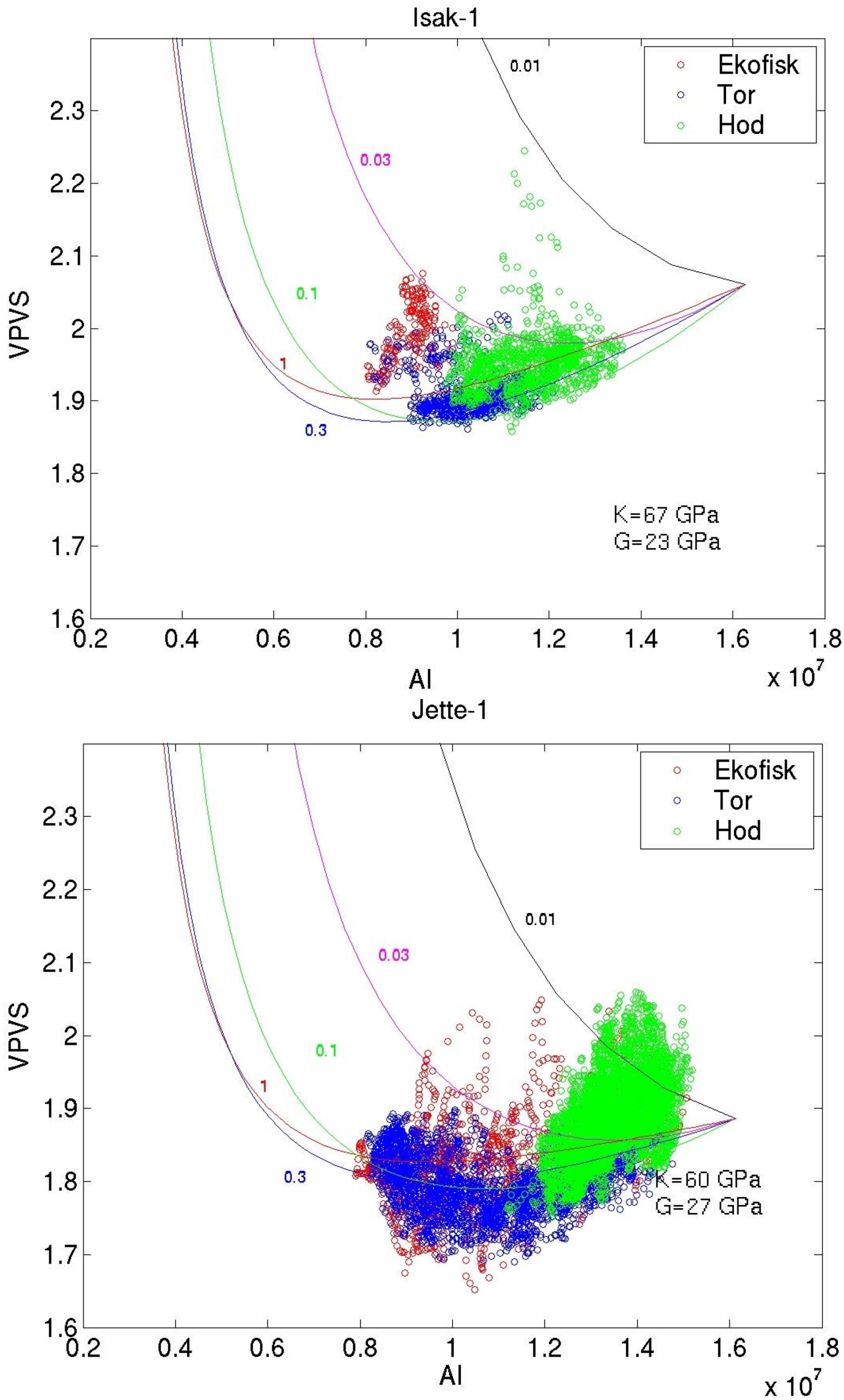

Figure 18. *Log Vp/Vs vs. acoustic impedance in Isak-1 and Jette-1. Ekofisk Formation is highlighted in red, Tor in blue, and Hod in green. Ellipsoidal pore models are superimposed.*

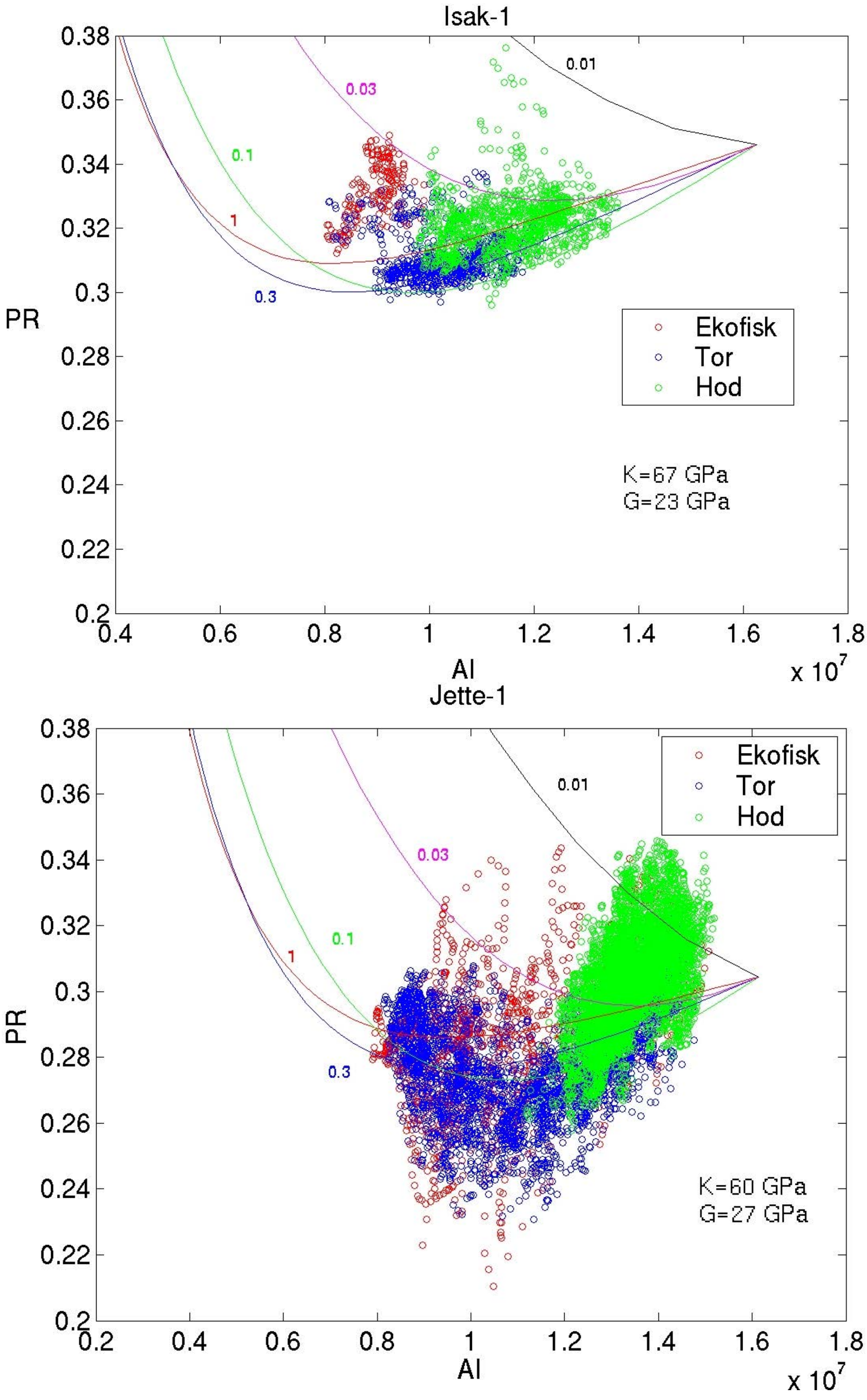

Figure 19. *Log Poisson's ratio vs. density porosity in Isak-1 and Jette-1. Ekofisk Formation is highlighted in red, Tor in blue, and Hod in green. Ellipsoidal pore models are superimposed.*

Summary

Differences between the sonic log data from wells Jette-1 and Isak-1 have been observed in the chalks of the Ekofisk, Tor, and Hod Formations. Both P- and S-wave velocities in Jette-1 tend to be larger than in Isak-1, while the Vp/Vs ratio is smaller in Jette-1. Comparison with rock physics ellipsoidal pore models suggest that the chalk in Jette-1 have stiffer pores than in Isak-1 and that the mineral end-point properties are different for the two wells. The moduli were adjusted empirically to find model predictions consistent with both P- and S-wave velocity data because the ellipsoidal inclusion model is very sensitive to the choice of mineral properties. The mineral moduli for Isak-1 were found to be K=67 GPa, G=23 GPa and those for Jette-1 K=60 GPa, G=27 GPa. Taking the properties of the Isak-1 mineral as the calcite end-member, the Jette-1 properties correspond to the theoretically expected value for a mixture of 80% calcite and 20% quartz. If the quartz fills the thinnest cracks and grain contacts the result would be a more rigid pore space and thus explain that the chalk in Jette-1 have stiffer pores than in Isak-1. The clean Tor Formation has little variation with gamma ray, whereas the clay-bearing Ekofisk and Hod Formations have a large variation in gamma ray and a corresponding spread in Vp vs porosity (apparent aspect ratios). This spread thus probably reflects the presence of clay, rather than a systematic change in pore shape. Velocities in Isak-1 increase monotonically with depth without a significant change of pore shape (porosities decreasing from 25% to less than 10%), while in Jette-1 the velocities are not well correlated with depth.

References

Berryman, J.G., 1995, Mixture theories for rock properties, *in: A Handbook of Physical Constants,* Ahrens, T.J., ed., American Geophysical Union, Washington, 236 pp.

Gassmann, F., 1951, Uber die elastizitat poroser medien, *Vier. der Natur Gesellschaft*, 96, 1-23.

Greenberg, M.L. and Castagna, J.P., 1992, Shear-wave velocity estimation in porous rocks: theoretical formulation, preliminary verification and applications, *Geophysical Prospecting*, 40, 195-209.

Tsuneyama, F., Nishida, A., Okamura, H., 2003, Vp/Vs as a rock frame indicator for a carbonate reservoir, First Break, 21, 22-27.